Converted-wave (*P-S*) prestack migration and migration velocity analysis

Shaowu Wang, John C. Bancroft, Don C. Lawton, and Darren H. Foltinek

ABSTRACT

Based on the consideration of prestack migration by equivalent offsets and common scatter point (CSP) gathers, a new approach for converted-wave prestack migration and velocity analysis is proposed. The theories for converted-wave prestack migration and migration velocity analysis are described. The equivalent offset is depth- and velocity-dependent. Velocity error has an effect on the equivalent offset, especially at the early time, but with the increasing time or depth, this effect becomes negligible. By resorting the data into the common conversion scatter point (CCSP) gathers with equivalent offset, this new method is very simple and fast.

In CCSP gathers, the relationship between the two-way travel time and equivalent offset is proven to be hyperbolic making the conventional *P-P* velocity analysis tool suitable to *P-S* velocity analysis. This provides a simple but powerful way to perform converted-wave migration velocity analysis and simplify the *P-S* processing.

The creation of a CCSP gather and its velocity analysis are fairly insensitive to the velocity error. Moreover, the velocity analysis is convergent when the initial velocity estimation is inaccurate, and the convergence rate is rapid.

The feasibility of the new algorithm was demonstrated by physical modeling data, numerical modeling and field data examples. The numerical modeling example proves the ability of dealing with a depth-variant velocity model, and also the ability of imaging dipping reflector using converted waves. The real data example shows the possible improvement of signal-to-noise ratio, as well as the improvement of velocity analysis and the images of the seismic events, while not reducing the bandwidth.

INTRODUCTION

Including converted-waves (*P-S*) in seismic surveys can provide for more fully integrated interpretation than that obtainable from *P-P* data alone. Recently, with increasing interest in petrophysics and 3-D subsurface structure determination by seismic exploration, people have been giving more attention to 3-D converted-wave seismic exploration (Tatham and Stewart, 1993). To facilitate this, a 3-D *P-S* processing flow, which differs from *P-P* data processing, must be established, and several new processing algorithms must be developed. Lawton and Wang (1994) established and evaluated a 3-D *P-S* processing flow in an isotropic medium using physical modeling data. Cary (1994) described a processing flow for 3-D converted-wave seismic data processing in an anisotropic medium, and successfully applied it to real data processing. Because the *P-S* ray paths are different from that of *P-P* waves, the corresponding *P-S* processing flow is different from *P-P* processing, and is more complex. Some special processing, such as birefringence analysis, common conversion point (CCP) binning, *P-S* NMO correction and velocity analysis, *P-S* DMO and migration, must be involved. Is there any method to simplify *P-S* data processing? Is it possible to use some of the algorithms which are exclusively suitable to *P-P* data processing to process *P-S* data? Prestack migration by equivalent offsets and common conversion scatter point (CCSP) gathers may assist in the answer to some these questions (Bancroft and Wang, 1994).

Prestack migration by equivalent offsets and common scatter point (CSP) gathers, which is based on the principle of prestack Kirchhoff migration, has already successfully been applied to *P-P* data processing (Bancroft et al., 1994). In this method, CSP gathers are created for each migrated trace by replacing the common midpoint (CMP) gathers of conventional processing. Samples for each input trace are assigned an equivalent offset for each output scatter point position, then transferred into the appropriate offset bin of the CSP gather. By doing this, the prestack time migration is reduced to be a simple re-sort of the data into CSP gathers, and the velocity analysis on these CSP gathers becomes more effective, because the CSP gather has more fold and a larger maximum offset than conventional CMP gather has. The method proved to be simpler, faster and more flexible than the conventional approach.

Prestack migration by equivalent offsets and CCSP gathers may be more attractive for converted-wave processing. After the *P-S* data are transformed into CCSP gathers by equivalent offsets, the asymmetry of the *P-S* ray paths is "removed", and some algorithms, such as conventional NMO correction and semblance velocity analysis, can be applied to the CCSP gathered *P-S* data, and CCP binning is not necessary. In this paper, we describe the principle of *P-S* prestack migration by equivalent offsets and CCP gathers, and discuss the effect of the velocity uncertainty on the accuracy of the equivalent offsets. Then we explain how to perform *P-S* migration velocity analysis using the conventional semblance velocity analysis tools. Finally, applications to physical, numerical modeling data and field data are discussed to demonstrate the feasibility of this method.

THEORY

The equivalent offset for converted-waves

As shown in Figure 1 (2-D) and Figure 2 (3-D), h_s, h_r and h_e are the source, receiver and equivalent offsets from the CCSP surface location respectively. If we assume that the depth of common conversion scatter point (CCSP) is Z_0 and the *P*-wave and *S*-wave migration velocities at this depth are $V_{p\ mig}$ and $V_{s\ mig}$ respectively, then their migration velocity ratio is defined as

$$\gamma_{mig} = \frac{V_{p\ mig}}{V_{s\ mig}} \ . \tag{1}$$

Following Bancroft and Wang (1994), the equivalent offset for converted-waves is computed by equating the travel times from the source T_s and receiver T_r with the travel times from co-located source T_{es} and receiver T_{er}, i.e.

$$T_{es} + T_{er} = T_s + T_r \ . \tag{2}$$

It can be expressed as

$$\frac{\left(Z_0^2 + h_e^2\right)^{1/2}}{V_{p\ mig}} + \frac{\left(Z_0^2 + h_e^2\right)^{1/2}}{V_{s\ mig}} = \frac{\left(Z_0^2 + h_s^2\right)^{1/2}}{V_{p\ mig}} + \frac{\left(Z_0^2 + h_r^2\right)^{1/2}}{V_{s\ mig}} \ . \tag{3}$$

Substituting equation (1) into equation (3) and solving for the equivalent offset h_e gives:

$$h_e = \left[\frac{1}{(1+\gamma_{mig})^2} \left(\left(Z_0^2 + h_s^2\right)^{1/2} + \gamma_{mig} \left(Z_0^2 + h_r^2\right)^{1/2} \right)^2 - Z_0^2 \right]^{1/2} . \quad (4)$$

In equation (4), the equivalent offset h_e is expressed as the function of depth Z_0. In practice, we do not know depth Z_0, but we do know the two-way travel time T. Splitting equation (3) into two equations yields:

$$\frac{\left(Z_0^2 + h_e^2\right)^{1/2}}{V_{p\ mig}} + \frac{\left(Z_0^2 + h_e^2\right)^{1/2}}{V_{s\ mig}} = T , \quad (5a)$$

$$T = \frac{\left(Z_0^2 + h_s^2\right)^{1/2}}{V_{p\ mig}} + \frac{\left(Z_0^2 + h_r^2\right)^{1/2}}{V_{s\ mig}} , \quad (5b)$$

solving for the Z_0^2 from above equations gives

$$Z_0^2 = \frac{C_2^2 - 2C_1 \pm C_2 \left(C_2^2 + 4h_s^2 - 4C_1\right)^{1/2}}{2}, \quad (6a)$$

where C_1 and C_2 are the coefficients, which are

$$C_1 = \frac{T^2 V_{p\ mig}^2 + h_s^2 - \gamma_{mig}^2 h_r^2}{1 - \gamma_{mig}^2}, \quad (6b)$$

$$C_2 = \frac{2TV_{p\ mig}}{1 - \gamma_{mig}^2}. \quad (6c)$$

By ensuring the value of Z_0^2 is real and positive, a unique solution of Z_0^2 in equation (6a) can be obtained. Substituting equation (6a) into equation (5a), and solving for h_e gives:

$$h_e = \left[\frac{T^2 V_{p\ mig}^2}{(1+\gamma_{mig})^2} - Z_0^2 \right]^{1/2} . \quad (6d)$$

Equations (6) are used to calculate equivalent offsets. For 3-D converted-waves, as shown in Figure 2, the co-location E for this particular R and S can be at any position on the circle with center at CCSP and radius h_e. Therefore in a 3-D *P-S* CCSP gather, azimuth distribution is not taken into account. Because of this, we call it a pseudo 3-D *P-S* CCSP gather.

The effect of velocity uncertainty on the accuracy of equivalent offset

In equations (6), it is shown that the equivalent offset h_e is the function of two-way travel time T, so it is depth-variant. We also notice that the expression of h_e is velocity-dependent. Because of these, it is necessary to know how sensitive the equivalent offset is to the velocity error and what is the effect of the velocity error on the accuracy of equivalent offset h_e.

Shown in Figure 3b are the h_e curves at different CCSP surface locations, calculated using the equations. Figure 3a shows the geometry of the source, receiver and CCSP surface positions in the source-receiver direction. In each curve, the start time is given by:

$$T_{start} = \frac{h_s}{V_{p\ mig}} + \frac{h_r}{V_{s\ mig}} = \frac{h_s}{V_{p\ mig}} + \frac{\gamma_{mig} h_r}{V_{p\ mig}}. \tag{7}$$

In Figure 3b, it is seen that when the CCSP surface position is exactly at the midpoint between the source and receiver, h_e is time- and velocity-independent and equal to the source to receiver offset. As the CCSP surface position moves away from the source-receiver midpoint, the variation of h_e with time or depth becomes faster. When the CCSP surface position is close to the source or receiver position, the fastest variation of h_e with time occurs. With the CCSP location further away from the midpoint, the change becomes slower again. As expected, the h_e curves are not symmetric along the midpoint because the asymmetry of the *P-S* ray paths. In this example, the source-receiver offset is quite large, reaches 4000 m, so the depth-dependent property of h_e is significant. Generally speaking, for a conventional migration aperture, h_e does not change very fast with time; for instance, when the CCSP is located between 1000 m and -1000 m. Figure 4 shows how the velocity error affects the equivalent offset h_e. Beside each curve is the relative velocity error. From this figure, it is seen that the velocity error indeed has some effect on h_e, especially at early times, but with increasing time, this effect becomes negligible. If the target depth is not shallower, this equivalent offset error should be within half of the offset bin increment for a reasonable velocity error.

Practical computation of the equivalent offset

The calculation of h_e based on the equations (6) is not very practical because the samples are moved to their equivalent offset bins sample-by-sample, and hence it is time consuming. In practice, the equivalent offsets are quantized into equivalent offset bins, as shown in Figure 5. A number of samples may have offsets that fall in the same offset bin. An improved procedure starts by computing the first offset with equations (6), then computes the time T_n when the following samples will be located in the next offset bin.

For a given h_{en}, $V_{p\ mig}$, γ_{mig}, h_s and h_r, solving for Z_{0n}^2 from equation (3) gives

$$Z_{0n}^2 = \frac{h_s^2 h_r^2 - b_n^2}{2b_n - h_s^2 - h_r^2}, \tag{8a}$$

where b_n is an intermediate value, i. e.

$$b_n = \frac{(1+\gamma_{mig})^2 h_{en}^2 - h_s^2 - \gamma_{mig} h_r^2}{2\gamma_{mig}}. \tag{8b}$$

Substituting Z_{0n}^2 into equation (5b), we get

$$T_n = \frac{\left(Z_0^2+h_s^2\right)^{1/2} + \gamma_{mig}\left(Z_0^2+h_r^2\right)^{1/2}}{V_{p\ mig}}. \tag{8c}$$

Instead of using equations (6), equations (8) are used to move the sample blocks to the appropriate offset bins.

PRESTACK MIGRATION VELOCITY ANALYSIS OF *P-S* WAVES

Velocity analysis for converted-waves is much more complicated than that for *P-P* waves, because its normal moveout (NMO) is non hyperbolic. A time-shifted hyperbolic NMO equation (Slotboom, et al., 1989; Slotboom, 1990) is needed to implement *P-S* NMO correction and *P-S* velocity analysis, but the time-shifted hyperbolic NMO equation is still just an approximation.

Very fortunately, in CCSP gathers, the relationship between the two-way travel time and equivalent offset as expressed in equation (5a) is actually hyperbolic. This makes us able to use conventional velocity tools to perform *P-S* migration velocity analysis. From equation (5a),

$$\begin{aligned} T &= \frac{\left(Z_0^2+h_e^2\right)^{1/2}}{V_{p\ mig}} + \frac{\left(Z_0^2+h_e^2\right)^{1/2}}{V_{s\ mig}} \\ &= \left(\frac{(1+\gamma_{rms})^2 Z_0^2}{V_{p\ mig}^2} + \frac{(1+\gamma_{mig})^2 h_e^2}{V_{p\ mig}^2}\right)^{1/2}, \end{aligned}$$

The above equation can be expressed as following form

$$T^2 = T_0^2 + \frac{(2h_e)^2}{V_{sem}^2}, \tag{9a}$$

with

$$T_0 = \frac{(1+\gamma_{mig})Z_0}{V_{p\ mig}}, \tag{9b}$$

and

$$V_{sem} = \frac{2V_{p\ mig}}{1+\gamma_{mig}}, \tag{9c}$$

where V_{sem} means the semblance velocity obtained from the velocity spectrum on the CCSP gathers using conventional velocity analysis tools. It has the same migration velocity form given by Eaton and Stewart (1991), i.e.

$$V_m = \frac{2V_pV_s}{V_p+V_s} = \frac{2V_p}{1+\gamma}.$$

From the *P*-wave migration velocity analysis in CSP gathers, $V_{p\ mig}$ can be obtained. Then, from equation (9c), the migration velocity ratio γ_{mig} and the migration *S*-wave velocity can be calculated by

$$\gamma_{mig} = \frac{V_{p\ mig}}{V_{s\ mig}} - 1, \tag{10a}$$

and

$$V_{s\ mig} = \frac{V_{p\ mig} V_{sem}}{V_{p\ mig} - V_{sem}}. \tag{10b}$$

THE RELATIONSHIP OF MIGRATION VELOCITY WITH RMS AND AVERAGE VELOCITIES

According to Dix equation, the travel time from source to common conversion scatter point (CCSP), as shown in Figure 1, can be expressed as

$$T^2 = T_0^2 + \frac{h^2}{V_{rms}^2}, \tag{11}$$

where h can be h_s or h_r, V can be V_p or V_s, and T_0 is the zero-offset travel time, it is the function of depth and average velocity, as shown in the following equation

$$T_0 = \frac{Z_0}{V_{ave}}. \tag{12}$$

As discussed in equation (3), if we express the travel time T as the function of depth, offset and migration velocity, then it is

$$T^2 = \frac{Z_0^2 + h^2}{V_{mig}^2}. \tag{13}$$

By substituting equations (12) and (13) into equation (11) and simplifying it, we have

$$V_{mig}^2 = \frac{\left(1 + \frac{h^2}{Z_0^2}\right) V_{rms}^2 V_{ave}^2}{V_{rms}^2 + \frac{h^2}{Z_0^2} V_{ave}^2}. \tag{14}$$

From the above equation, the migration velocity is generally not only the function of RMS and average velocities, but also the function of offset and depth. For a constant velocity model, migration velocity is the same as RMS velocity and average velocity. But if the velocity function is depth-variant, it is very complex and depends on the geometry and time (or depth). Based on the analysis of the equation (14), the following asymptotic features can be derived,

when $\frac{h_s}{Z_0} \to 0$, $V_{mig} = V_{ave}$ and

when $\frac{h_s}{Z_0} \to \infty$, $V_{mig} = V_{rms}$.

These equations show us that the migration velocity is close to average velocity at early times, while it is close to the RMS velocity at later times. For any time, offset and velocity model, the migration velocity is therefore between the average and RMS velocities. The following table calculated from a simple layered model also demonstrates these conclusions.

Table1. Average and RMS and migration velocities at different depths for a given velocity model. The calculation is based on equation (14) with h of 1000 m.

depth (m)	interval vel. (m/s)	average vel. (m/s)	RMS vel. (m/s)	migration vel. (m/s)
200	3000	3000.00	3000.00	3000.00
500	3200	3059.21	3059.93	3059.79
1000	3400	3175.05	3177.49	3176.49
1150	3500	3208.40	3212.18	3210.03
1200	2900	3208.05	3211.87	3209.61
1600	3400	3193.34	3197.13	3194.40
2000	3600	3250.29	3255.61	3251.35
2500	3800	3331.27	3340.09	3332.48
10000	4000	3740.36	3751.60	3740.47

APPLICATIONS AND DISCUSSION

3-D 3-C physical modeling example

The new algorithm was first applied to physical modeling data. The model consists of a rectangular-shaped cavity milled into the base of a layer of plexiglas of 9.8 cm thick, with *P*-wave velocity of 2750 m/s and *S*-wave velocity of 1375 m/s. The cavity is about 1.4 cm deep, 8.0 cm long, 5.0 cm wide and is air-filled. World units are shown using a distance scaling factor of 10,000:1. The cross-sections of the model are shown in Figure 6.

A 3C-3D data set was acquired over the model using a *P*-wave transducer as the source. A plan view of the survey is shown in Figure 7, with all dimensions shown after a distance scaling factor of 10,000:1 has been applied. There were 7 shot lines with line spacing of 200 m, 19 shots per shot-line and shot spacing of 50 m. For each

shot, data were acquired along 10 receiver lines with a spacing of 100 m, a near offset of 200 m, 18 receiver stations per receiver line and a receiver spacing of 50 m. The sample rate was 1 ms and the record length was 1.5 s. The survey was repeated three times to enable vertical, in-line and cross-line receiver components to be collected. Here, in-line refers to receiver-line direction and cross-line refers to shot-line direction.

Figure 8 is an example of a CCSP gather and its velocity spectrum using a conventional velocity analysis. In the left panel of Figure 8, the event at 1100 ms is the *P*-*S* reflection from the bottom of the model, whereas the event at 740 ms is *P*-wave leakage. In this example, it is seen that *P*-*S* event, which is non-hyperbolic in conventional CCP gather appears to be hyperbolic in CCSP gather. This property is clear in the velocity spectrum, in which the velocity semblance is highly focused. However, in Figure 9, because the *P*-*S* event in a conventional CCP gather is not hyperbolic, the velocity spectrum is smeared due to the assumed hyperbolic NMO equation to calculate the velocity spectrum.

Figures 10 and 11 are the example sections of *P*-*S* migrated data in receiver-line direction using conventional *P*-*S* processing flow and the new method discussed in this paper, respectively. Details were discussed in the paper by Lawton and Wang (1994). The post-stack migration applied to the data in Figure 10 was single-pass phase-shift migration. In Figure 11, only the central part of the section is plotted. Careful comparison of these two figures shows that the prestack migrated section is better than the poststack migrated section in the imaging of the 3-D structure and ability to collapse diffractions.

In this physical model example, the effect of the velocity error on the CCSP gather and velocity analysis result was tested. Table 2 shows how the velocity error in the calculation of the equivalent offset affects the velocity analysis.

Table 2. The effect of *S*-wave velocity error in the calculation of equivalent offset on the result of migration velocity analysis.

V_p (m/s)	V_s (m/s)	V_s error (%)	V_{sem} (m/s)	V_s (m/s) From V. A.	relative error (%)
2750	1375	0 %	905	1349	1.9 %
2750	1237.5	-10 %	894	1324	3.7 %
2750	1100	-20 %	889	1314	4.4 %
2750	825	-40%	789	1106	19.6 %

In this test, the *P*-wave velocity was kept unchanged while the *S*-wave velocity was changed. From this table, it is known that when the velocity error is less than 20 %, reasonably accurate velocity result can still be obtained. This means that the CCSP gather and velocity analysis are fairly insensitive to the velocity error. In practice, after the velocity function is obtained by the velocity analysis on a CCSP gather, the output velocity function can be input to update the equivalent offset CCSP gather and the velocity analysis can be repeated. Very importantly, the updated velocity function is convergent and through this iteration procedure, an accurate velocity function can finally be reached.

Numerical modeling example

In the above example, the model has a constant velocity. To demonstrate the feasibility of the *P-S* migration velocity analysis, it is necessary to deal with a depth-variant velocity model. Due to this motivation, we created a synthetic data set using ray-tracing software. As shown in Figure 12, the model consists of four layers with depth variant velocities (*Vp* and *Vs*) and velocity ratio (γ). On the third interface, there are two symmetric dip angle of 30 degrees. The *P*- and *S*-wave velocities and the depth of each layer are shown in this figure. The prestack data set consists of 75 shots with shot interval of 40 m. There are 100 receivers for each shot with receiver interval of 40 m. The prestack migration program was converted into ProMax compatible code and modified to deal with depth-variant velocity model. Figures 13 (a) and (b) are two typical examples of CCSP gathers. The CCSP gather in Figure 13 (a) is located at CCSP surface location number 20, which is above the flat part of the third layer, while another CCSP gather (b) is at 40, which is above the dipping reflector. In these two figures, the *P-S* reflection events, whether from the flat reflectors or from the dipping surface, appear to be hyperbolic. This is very clear in Figure 14, in which the velocity spectrum is highly focused. Another important feature obtained from Figure 13 (b) is that the reflection energy from a dipping reflector occurs mainly over the medium and far offset. Figure 14 shows the effectiveness of migration velocity analysis on the CCSP gathers discussed in this paper. Although the location for the velocity analysis is at the location of dip change, as shown in the stacked panel in this Figure, a very accurate single velocity value can still be obtained. The velocity field distribution is also coincident with the model. Figure 15 shows the comparison of the theoretical *P-S* RMS and migration velocities with velocity analysis results after different velocity analysis iteration. Because the *P-S* migration velocity function in the creation of the CCSP gathers is not known, we generally begin with a constant *P-S* migration velocity value (initial velocity) to form the CCSP gathers. Then, by performing velocity analysis on these CCSP gathers, a velocity function (velocity after 1st iteration) is obtained. After repeating this procedure, the velocity function (velocity after 2nd iteration) is quite close to the theoretical RMS or average *P-S* velocities. This means the prestack migration and migration velocity analysis result are rather insensitive to the velocity error, and are convergent. The *P-S* stacked section in Figure 16 demonstrates that this method can successfully migrate the dipping reflections to their true positions and collapse the diffractions. Very interestingly, at the two dip conflicting points A and B, as shown in Figure 16, there are two diffration evidents. They seem to be migration 'noise', this is due to the fact that ray tracing fails to simulate the diffractions at these points.

Lousana multicomponent seismic data example

In the physical and numerical modeling examples, the signal-to-noise ratio (S/N) is very high, or noise free, and the geometry is regular. This is rarely true in real data. As the last step to demonstrate the new algorithm, it was applied to multicomponent seismic data from Lousana, Alberta. Data acquisition and previous processing were discussed in greater detail by Miller et al. (1993, 1994). The poststack migrated *P-S* section processed on the ProMax system in 1994 for Line EKW-002 is shown in Figure 19. *P-S* migration velocity analysis on conventional CCP super gather is shown in Figure 17, while the migration velocity analysis on CCSP gathered data using conventional *P-P* velocity analysis tool is shown in Figure 18. Although a CCP super gather with 9 CCP gathers was formed to perform velocity analysis in Figure 17, the result in Figure 18 is still better than in Figure 17. This improvement can be seen in the highly focused velocity semblance, and signal-to-noise ratio appears to be higher.

The *P-S* stacked for Line EKW-002 after prestack migration is shown in Figure 20. Compared with Figure 19, the bandwidth in this Figure is approximately the same, but the Viking horizon (the peak at about 1550 ms) and the Nisku event (the peak at about 1990 ms) seem to be improved and signal-to-noise ratio also appears to be higher. The result in Figure 20 seems more interpretable than in Figure 19.

CONCLUSIONS

Based on the above applications and discussions, following conclusions can be obtained:

1. The theories for converted-wave prestack migration and velocity analysis were described. The equivalent offset is not only depth-dependent but also velocity-dependent. The depth-dependent characteristic of the equivalent offset becomes significant when the CCSP surface location is close to the source or receiver. Velocity error has effect on equivalent offset, especially at early times, but with increasing time or depth, this effect becomes negligible.

2. This prestack migration and migration velocity analysis can simplify the *P-S* processing, as well as improve the image of the *P-S* reflections. By resorting the data into the CCSP gathers with equivalent offsets, this new method is very simple and fast.

3. In CCSP gathers, the relationship between the two-way travel time and equivalent offset is hyperbolic. This makes conventional *P-P* velocity analysis suitable to *P-S* velocity analysis. This new approach provides a simple but powerful way to perform migration velocity analysis for converted-waves.

4. The algorithm is very stable. The CCSP gather and its velocity analysis are fairly insensitive to the velocity error and the velocity analysis is convergent and the convergence speed is fast. When the velocity error is as large as 40%, an accurate velocity function can still be obtained by a couple of iterations.

5. Physical modeling data, numerical modeling and field data examples demonstrated the feasibility of the new algorithm. The real data example shows not only the improvement of signal-to-noise ratio but also the improvement of velocity analysis and the imaging of the seismic reflection, while not reducing the bandwidth.

ACKNOWLEDGMENTS

We would like to acknowledge Unocal Canada Ltd. for donating the seismic data to the CREWES Project. We are grateful to Dr. R. R. Stewart for his helpful discussions. The financial support from the CREWES Sponsors is very appreciated.

REFERENCES

Bancroft, J. C., Geiger H. D., Foltinek, D. S., and Wang, S., 1994, Prestack migration by equivalent offsets and CSP gathers: CREWES project research report, v.6, 27.1-27.18

Bancroft, J. C., and Wang, S., 1994, Converted-wave prestack migration and velocity analysis by equivalent offsets and CCSP gathers: CREWES project research report, v.6, 28.1-28.7

Cary, P. W., 1994, 3-D converted-wave seismic processing: CREWES project research report, v.6, 31.1-31.10

Eaton, D.W.S. and Stewart, R.R., 1991, The Fresnel zone for *P-S* wave: Geophysics, v.56, 360-364

Miller, S. L. M., Harrison, M. P., Szata, K. J., and Stewart, R. R., 1993, Processing and preliminary interpretation of multicomponent seismic data from Lousana, Alberta: CREWES Research Report, v 5, 16.1-16.17

Miller, S. L. M., Harrison, M. P., Lawton, D. C., Stewart, R. R., and Szata, K. J, 1994, Analysis of *P-P* and *P-S* seismic data from Lousana, Alberta: CREWES Research Report, v 6, 7.1-16.24

Slotboom, R.T. and Lawton, D.C., 1989, Depth-variant mapping and moveout correction of converted-wave data: CREWES project research report, v.1, 55-67

Slotboom, R.T., Eaton, D.W., and Lawton, D.C., 1990, Improving converted-wave (*P-S*) moveout estimation: CREWES project research report, v.2, 80-88

Tatham, R.H., and Stewart, R.R., 1993, Present status and future directions of shear-wave seismology in exploration: CREWES project research report, v.5, 1.1-1.22

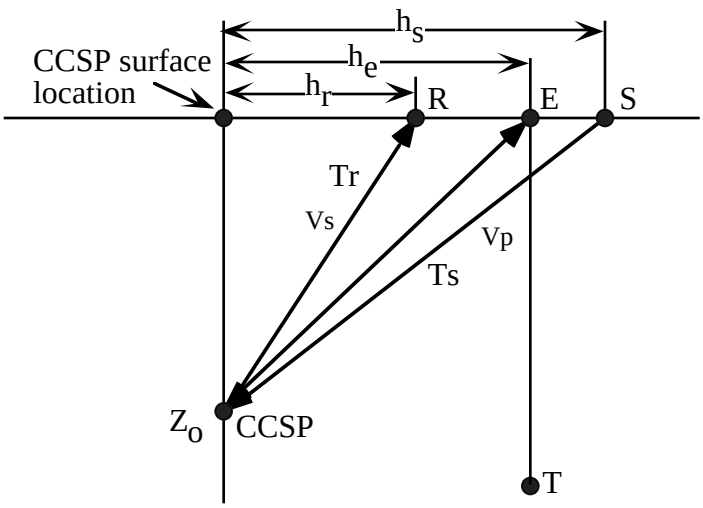

Fig 1. The ray paths and travel times for a common conversion scatter point and the position of the equivalent offset

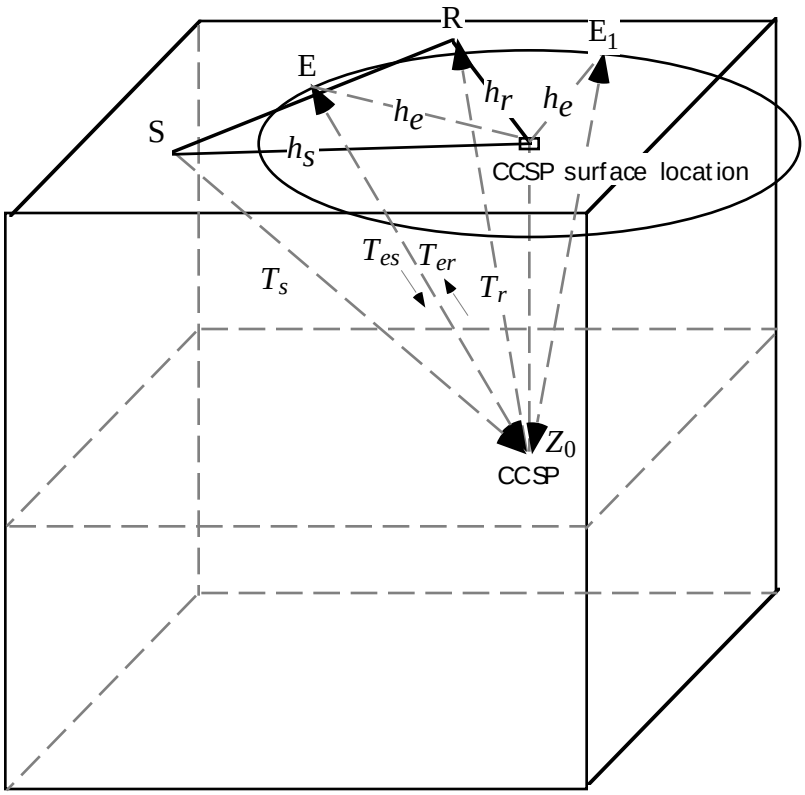

Fig. 2. Diagram showing the ray paths and travel times for a common conversion scatter point in a 3-D volume

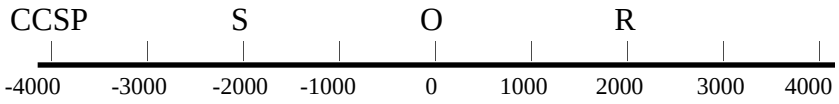

S: Source position
R: Receiver position
O: Midpoint of S to R

Vp=3000 m/s
Vs=1500 m/s
offset=4000 m

(a)

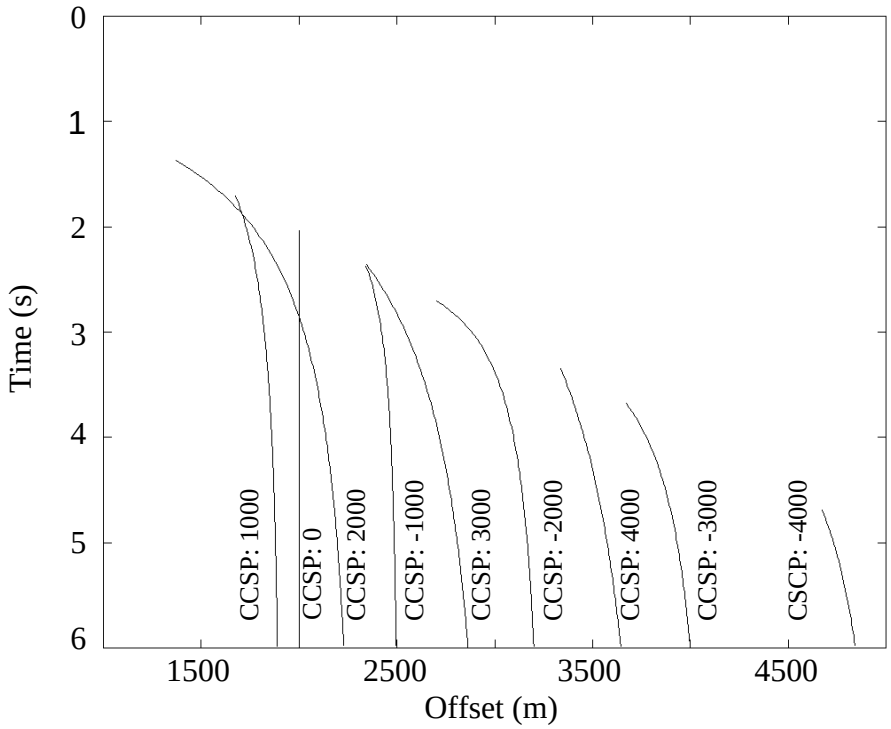

(b)

Fig. 3. The geometry of different CCSP locations on the surface (a) and the equivalent offsets at different locations as the function of time (b)

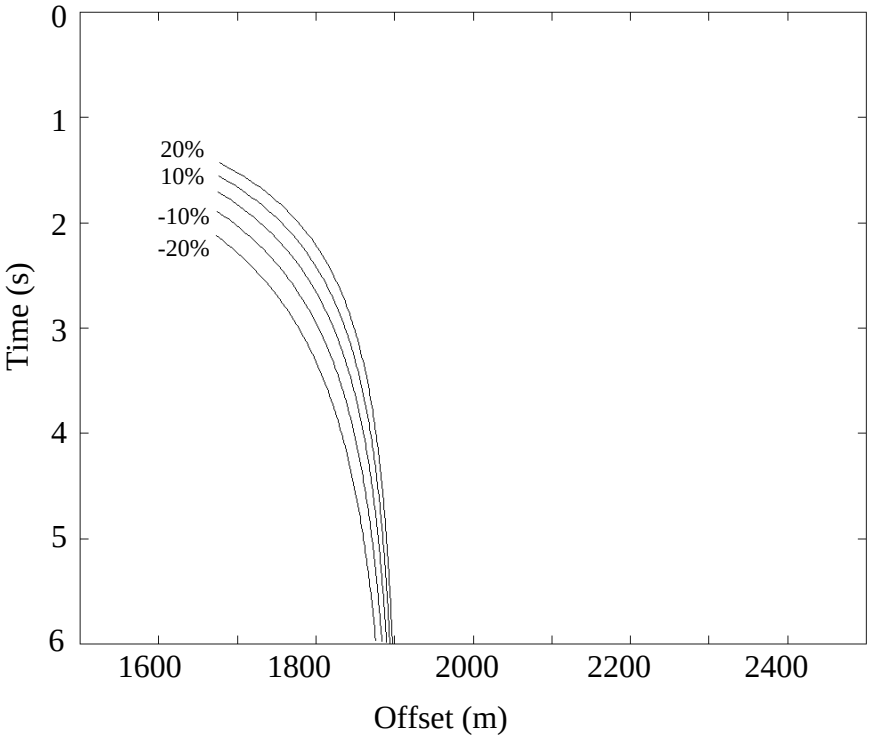

Fig. 4. The effect of velocity error on the accuracy of equivalent offset. The CCSP surface location is at 1000 m as shown in Figure 3a, and the other parameters are the same as in Figure 3a.

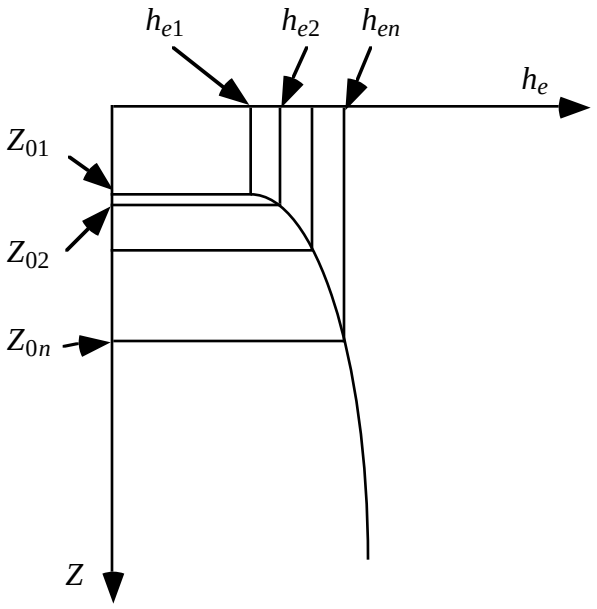

Fig. 5. Digram showing how to implement calculation of equivalent offset.

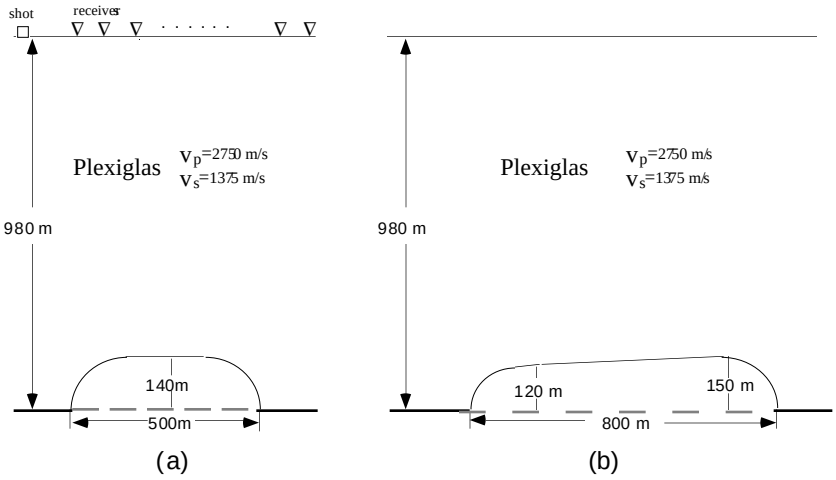

Fig. 6. Cross-sections of the model in receiver-line (a) and shot-line (b) directions across the center of the model.

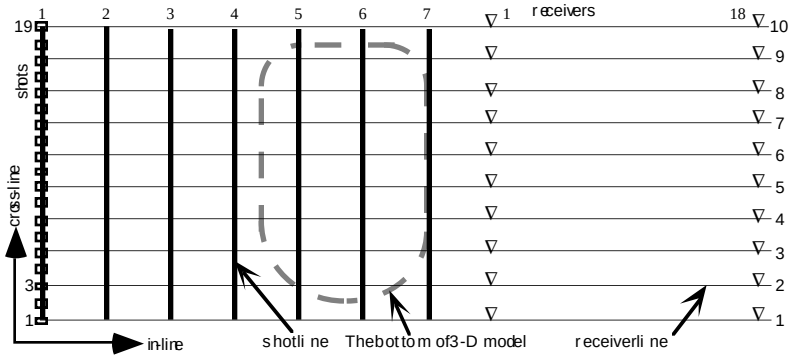

Fig. 7. Plan view of model showing acquisition geometry. Receiver locations are indicated for shot line #7.

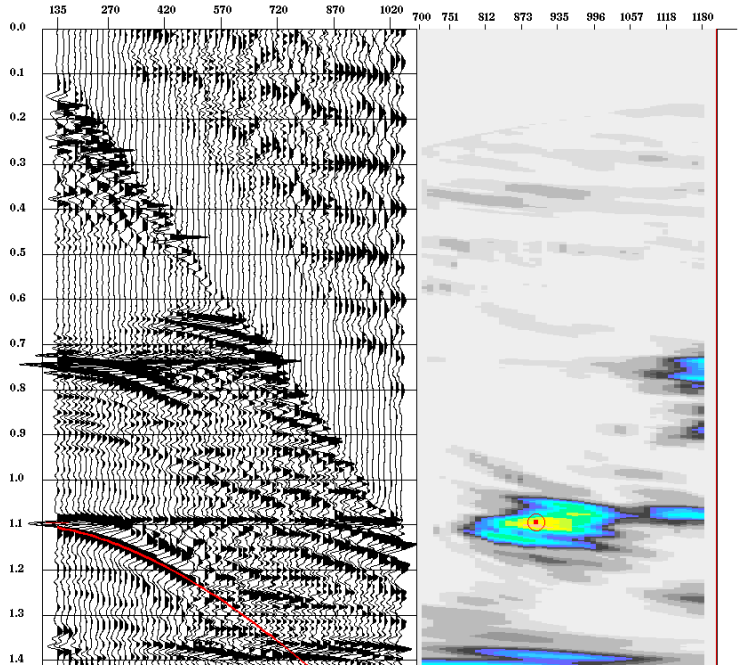

Fig. 8. The semblance velocity analysis of *P-S* CCSP gather using conventional velocity analysis method. Notice that in CCSP gather, *P-S* event is a hyperbola.

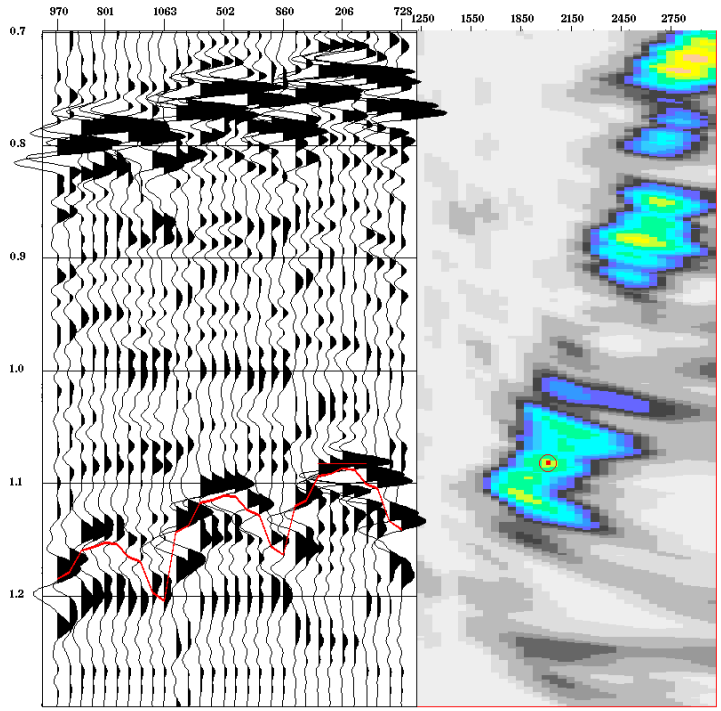

Fig. 9. The semblance velocity analysis of conventional CCP gather. Notice the smear of the semblance for the *P-S* event at time 1100 ms. This means that *P-S* event is not a hyperbola.

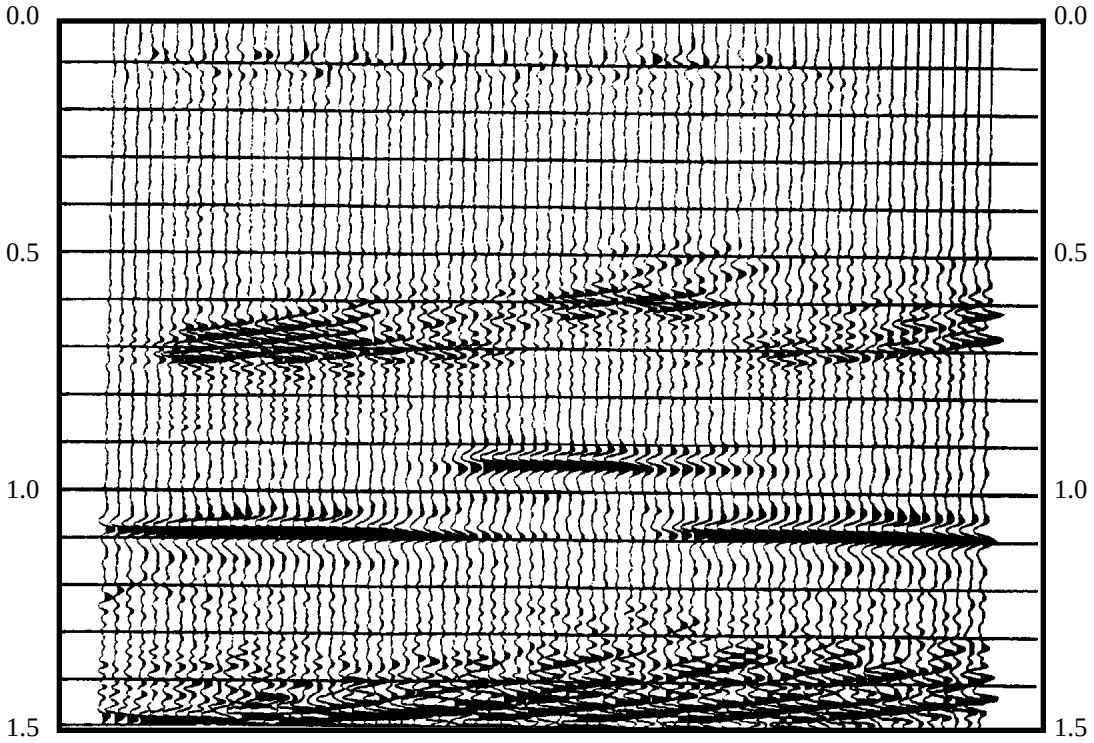

Fig. 10. Example section of *P-S* migrated data in receiver-line direction after interpolation of the empty traces

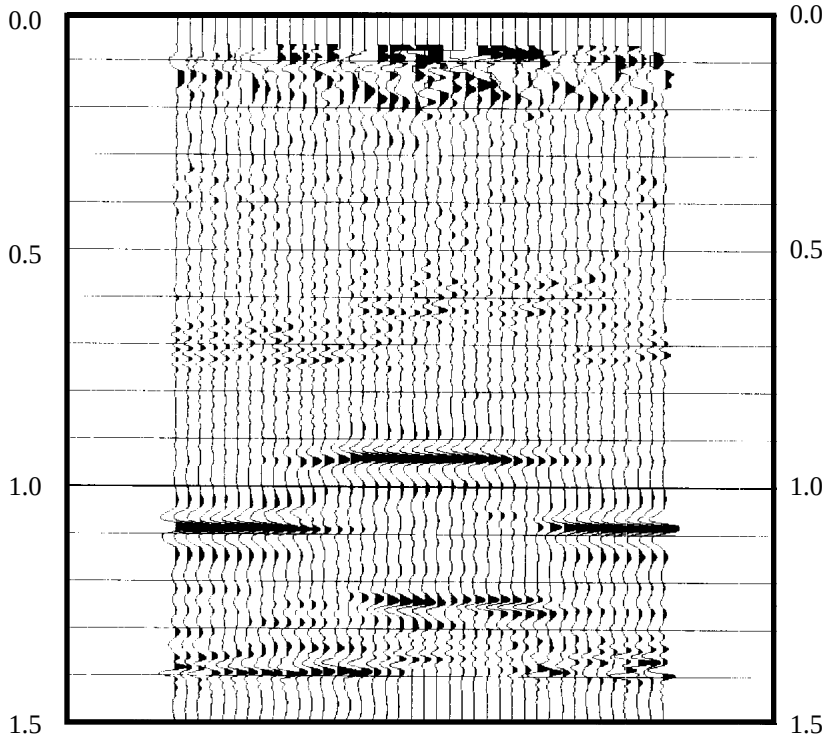

Fig. 11. Example section of *P-S* prestack migrated data in receiver-line direction using equivalent offsets and CCSP gathers.

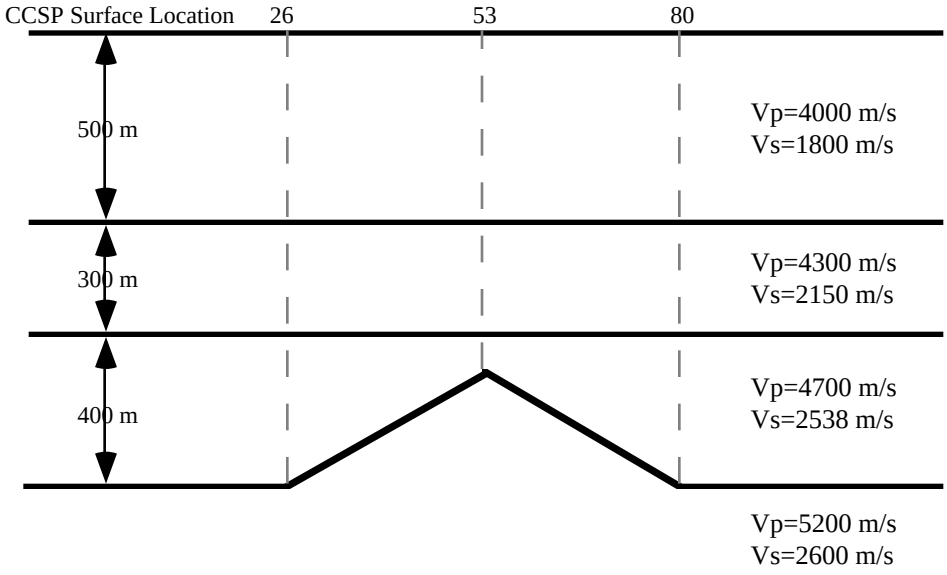

Fig. 12. Cross-section of the 4-layer model. The CCSP surface location interval is 20 m, and the dipping reflactors are symmetrical and their dipping angles are 30 degree.

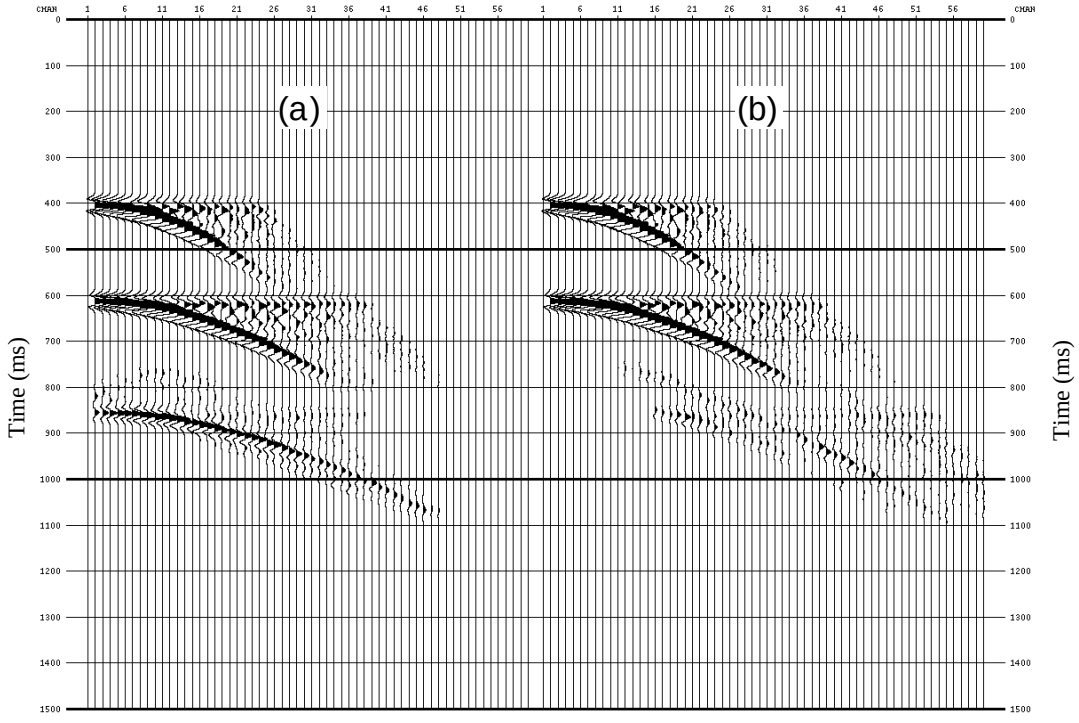

Fig. 13. Example of CCSP gathers. (a) is the CCSP gather with CCSP surface location at 20, which is located above the flat part of the third layer, while (b) is at 40, which is located above the dipping reflector.

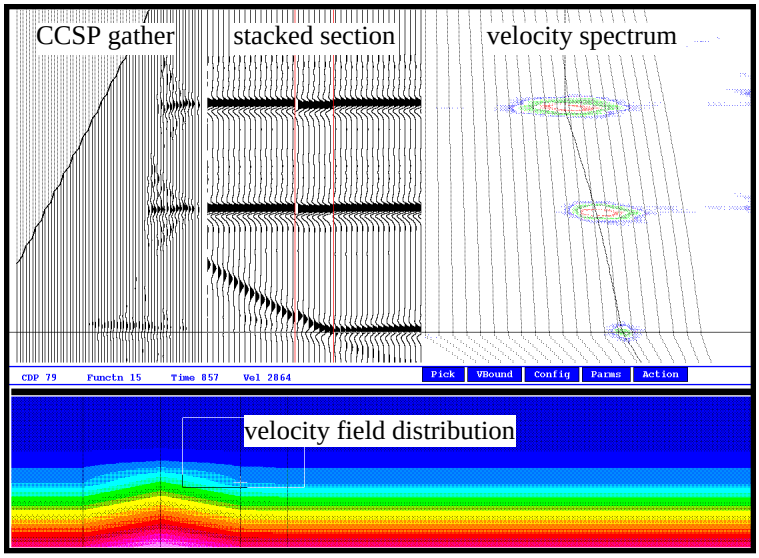

Fig. 14. *P-S* velocity analysis after CCSP gathering. The left upper is the stacked section; the right upper is the semblance velocity spectrum and the bottom is the velocity field distribution.

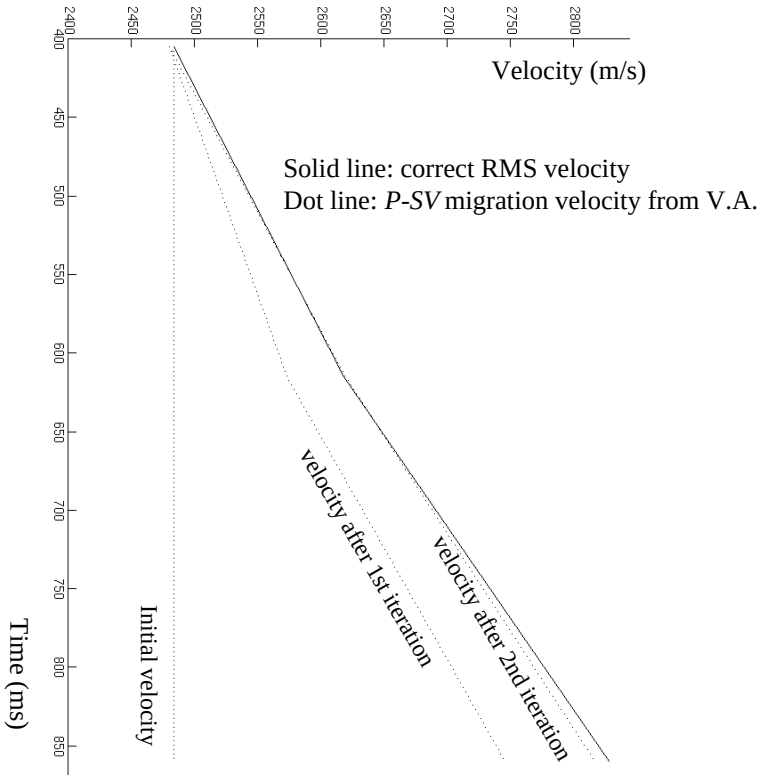

Fig. 15. The comparison of correct RMS velocity with velocity analysis results using the method discussed in the paper after different velocity analysis iterations

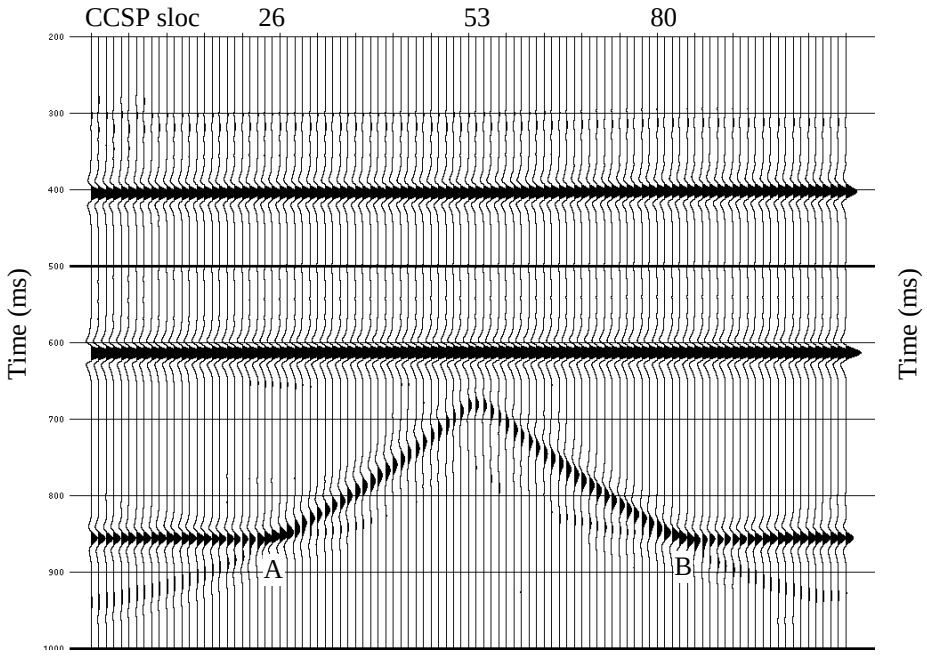

Fig. 16. *P-S* stacked section after *P-S* prestack migration

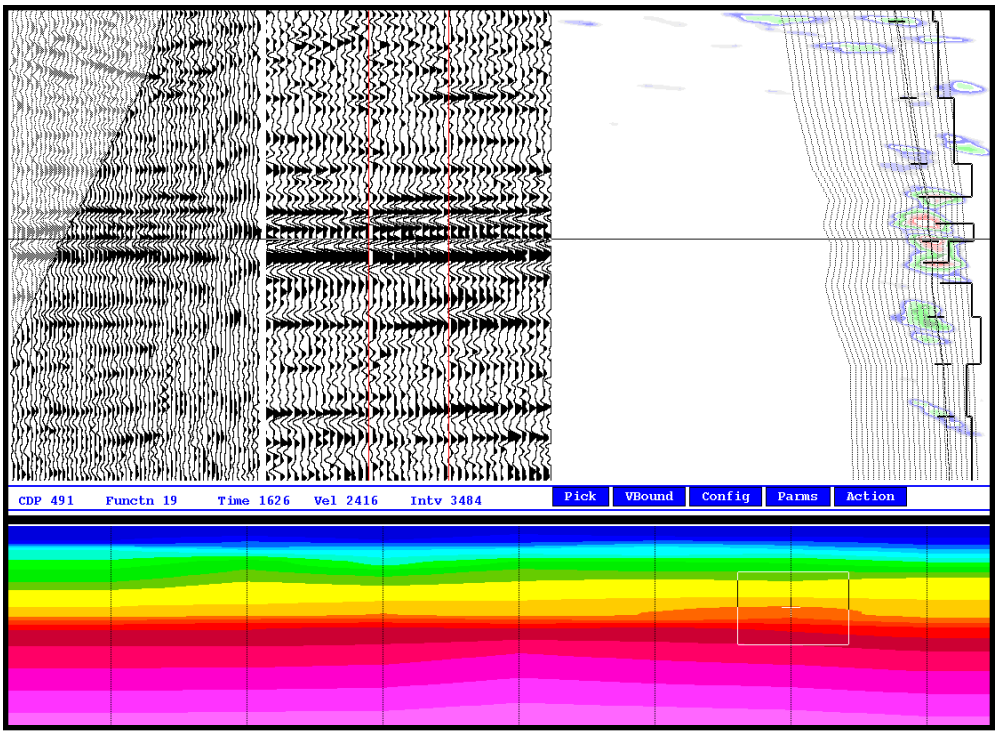

Fig. 17. *P-S* velocity analysis on conventional CCP super gather. The super gather consists of 9 CCP gathers.

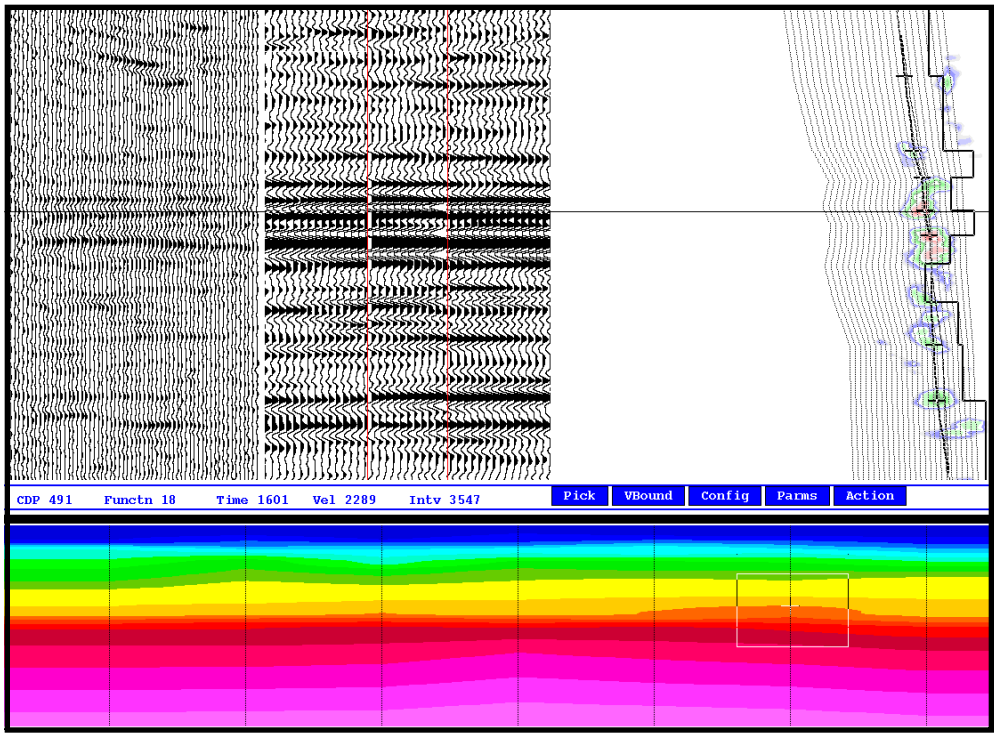

Fig. 18. *P-S* velocity analysis on CCSP gathered data discussed in the paper using conventional velocity analysis tool. Note more focused velocity semblance than in Figure 17 and improved signal-to-noise ratio.

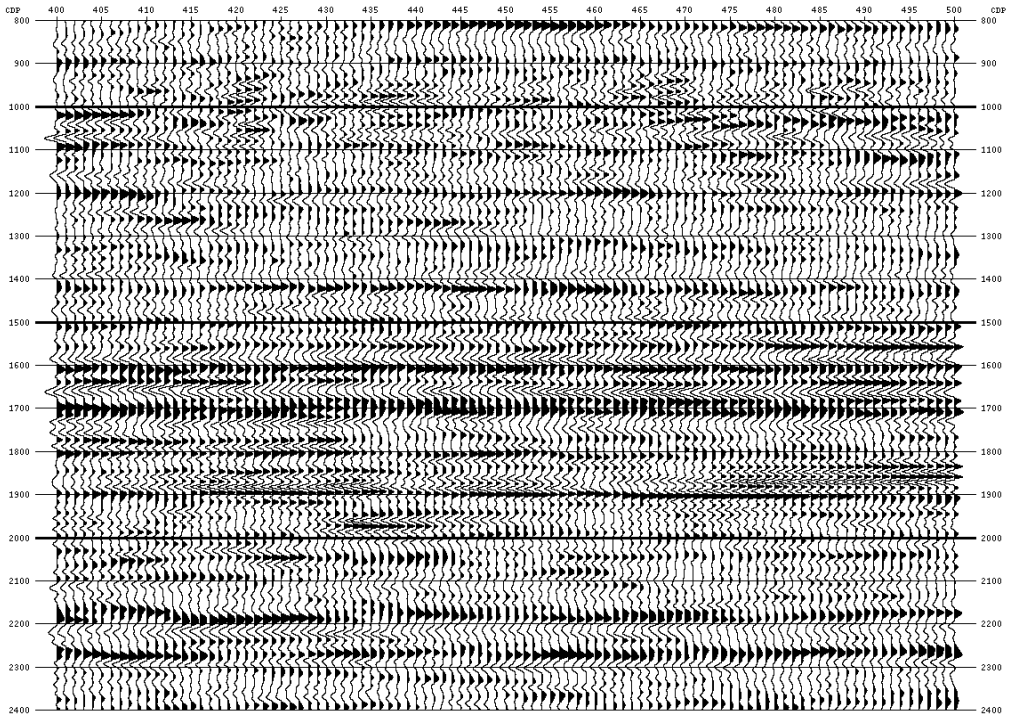

Fig. 19. The *P-S* migrated section for Line EKW-002 using conventional *P-S* processing flow on ProMax (1994).

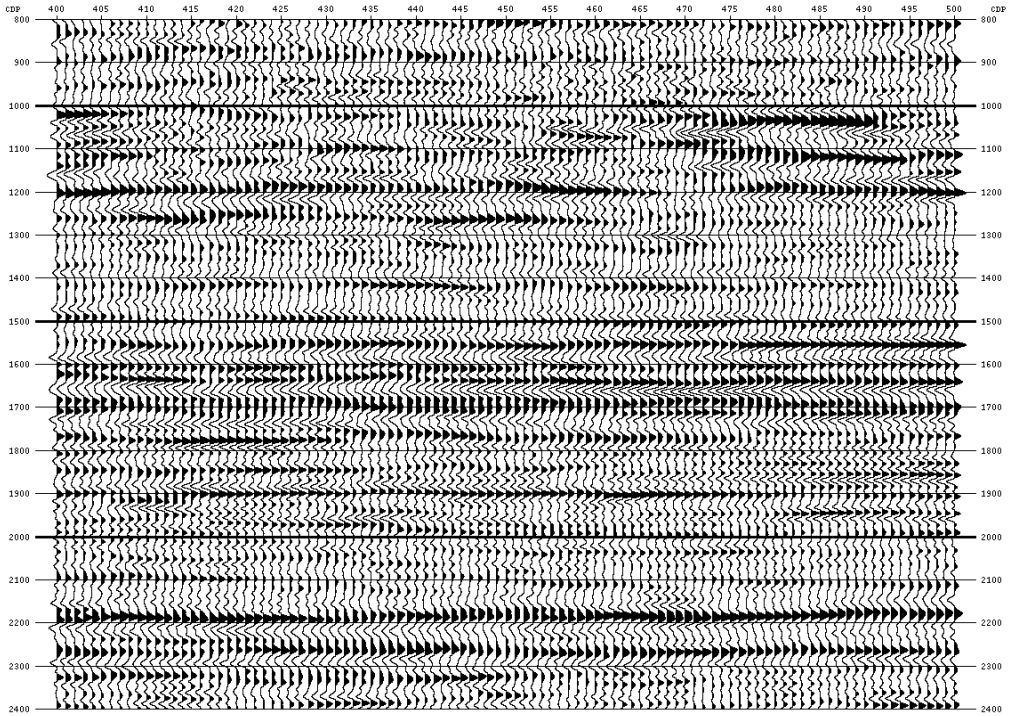

Fig. 20. The *P-S* stacked section for Line EKW-002 after CCSP gathering. Compared with Figure 19, it has almost the same bandwidth, but the imagings of the Viking horizon (the peak at about 1550 ms) and the Nisku event (the peak at about 1990 ms) are improved and also the signal-to-noise ration is improved.